AIP | Physics of Fluids

Dynamics of step-emulsification: From a single to a collection of emulsion droplet generators

Nitesh Mittal, Céline Cohen, Jérôme Bibette, and Nicolas Bremond

Citation: Physics of Fluids (1994-present) **26**, 082109 (2014); doi: 10.1063/1.4892949
View online: http://dx.doi.org/10.1063/1.4892949
View Table of Contents: http://scitation.aip.org/content/aip/journal/pof2/26/8?ver=pdfcov
Published by the AIP Publishing

PHYSICS OF FLUIDS **26**, 082109 (2014)

Dynamics of step-emulsification: From a single to a collection of emulsion droplet generators

Nitesh Mittal,[a] Céline Cohen,[b] Jérôme Bibette, and Nicolas Bremond[c]
Laboratoire Colloïdes et Matériaux Divisés, Institute of Chemistry, Biology and Innovation (CBI) ESPCI ParisTech, CNRS-UMR8231, PSL Research University, 10 rue Vauquelin 75231 Paris Cedex, France*

(Received 7 March 2014; accepted 28 July 2014; published online 19 August 2014)

Microfluidics has proven to be an efficient tool for making fine and calibrated emulsion droplets. The parallelization of drop makers is required for producing large amounts. Here, we investigate the generation of emulsion drops along a series of shallow microchannels emerging in a deep one, in other words the step-emulsification process. The dynamics of a single drop maker is first characterized as a function of interfacial tension and viscosities of both phases. The characteristic time scale of drop formation, namely, the necking time that finally sets drop size, is shown to be principally governed by the outer phase viscosity to interfacial tension ratio with a minor correction linked to the viscosity ratio. The step emulsification process experiences a transition of fragmentation regime where both the necking time and drop size suddenly raise. This transition, that corresponds to a critical period of drop formation and thus defines a maximum production rate of small droplets, is observed to be ruled by the viscosity ratio of the two phases. When drops are produced along an array of microchannels with a cross flow of the continuous phase, a configuration comparable to a one-dimensional membrane having rectangular pores, a drop boundary layer develops along the drop generators. In the small drop regime, the local dynamics of drop formation is shown to be independent on the emulsion cross flow. Moreover, we note that the development of the drop boundary layer is even beneficial to homogenize drop size along the production line. On the other hand, in the large drop regime, drop collision can trigger fragmentation and thus lead to size polydispersity.
 [http://dx.doi.org/10.1063/1.4892949]

I. INTRODUCTION

Emulsions, namely, metastable dispersions of liquid droplets into a second immiscible liquid phase with the presence of surface active agents, are a widespread material encountered in everyday life and industry from polymerization, paint, and road making applications, to cosmetics or food industries.[1] Numerous strategies based on mechanical energy input have been developed for producing emulsions. Most of them relies on a shear process where large drops are stretched and further fragmented in smaller droplets.[2] One can mention high pressure systems, rotor-stator, or disc systems as well as ultrasonic assisted processes. These typical emulsification techniques often lead to broad distributions of droplet size since the shear is not homogeneous. We note that the use of a Taylor-Couette geometry with a narrow and uniform gap allows to obtain monodisperse droplets thanks to a controlled shear over all the emulsion.[3] In addition, the final size distribution is governed by a competition between drop breakup and drop coalescence and the adsorption kinetics of surfactant at liquid-liquid interfaces must be considered.[4] Finally, producing calibrated emulsion

[a] Also at Ecole Polytechnique, Palaiseau Cedex 91128, France.
[b] Present address: UNSA University, CNRS UMR 7336, Parc Valrose, 06100 Nice, France.
[c] Author to whom correspondence should be addressed. Electronic mail: Nicolas.Bremond@espci.fr

droplets in the 1–10 μm range finds applications in biotechnologies. Indeed, for example, droplets can act as templates for making magnetic solid particles used in sample preparation,[5] sequencing,[6] or immunoassay.[7]

An efficient technique named membrane emulsification where the liquid to be dispersed flows through a porous material has been proposed in the early 1990s.[8–10] The drop size is scaled by the pore geometry,[8] as well as the shear flow of the continuous phase if any.[11,12] The polydispersity of the emulsion is mainly linked to pore size heterogeneities. Taking advantage of technological progresses of microfabrication, Nakajima and co-workers have designed an almost perfect one-dimensional membrane where the pores, that separate two deep reservoirs, are rectangular and shallow microchannels.[13] This process is known as microchannel emulsification or step emulsification. They further developed microfabricated membrane having elongated through-hole.[14,15] Here, the drop formation is a capillary driven phenomenon[16] triggered by the confinement release at the microchannel end, i.e., at a step height. There exists a critical aspect ratio of the microchannel of about 3 below which the step emulsification process fails.[17] The fact that the so-called Shirasu porous glass membrane, which is obtained from a phase separation of a glass synthesized from a volcanic ash called Shirasu,[8] leads to remarkable monodispersity might arise from the elongated shape of pores at the membrane surface.[8,18] In addition, the depth of the deeper channel after the step should be at least two times larger than the shallow microchannel height in order to obtain a drop size independent on step height.[19] The emulsification process exhibits a transition from the production of small to large drops when the dispersed phase flow rate is increased[20] as also observed in a co-flow situation.[21] Apart from a few investigations,[22] most of the experimental studies,[23] theoretical models,[24,25] or numerical simulations[26,27] on the step emulsification phenomenon consider microchannels with a widening end, and thus the presence of a terrace, prior to the height jump. In that case, a flatten drop having a discoidal shape is first form at the terrace before being fragmented in a smaller droplet. Microchannel dimensions and terrace length affect drop size and the transition of emulsification regime.[20,28] Despite numerous experimental investigations, a complete mapping of the drop formation dynamics as a function of liquid properties for a given microchannel geometry is still lacking. As initially intended for[13] this emulsification process is easily parallelized for producing large amount of fine and calibrated emulsions.[29] A flow of the continuous phase perpendicular to the microchannel array can be used for collecting emulsion droplets.[29,30] The emulsification dynamics in such a configuration, i.e., in presence of a cross flow of the continuous phase carrying on emulsion droplets, has not been studied in detail so far.

In this article, we report a parametric study on the features of step emulsification of newtonian fluids by varying their bulk and interfacial properties while keeping fixed the geometry of microchannels without any terrace and with a cross flow. The first part concerns the dynamics of a single drop generator where characteristic time scale of drop formation, drop size, and transition between two regimes of fragmentation are documented. The second part deals with an ensemble of drop generators which form a one-dimensional membrane with a cross flow. Their collective behavior in terms of emulsification dynamics and drop features is investigated.

II. MATERIALS AND METHODS

The microfluidic devices are fabricated by standard soft lithography techniques.[31] The photoresist mould is made by a two steps procedure that results in two channel depths. The ratio between the channel depths is here equal to 10. The mould is replicated by using poly-dimethylsiloxane (PDMS Sylgard, Dow Corning). Once cured, the elastomer replicate is bonded to a glass plate by using oxygen plasma that in addition become hydrophilic. The microsystem is finally heated for 10 min at 70 °C for improving the bonding strength and then filled with water within 30 min to ensure the PDMS channel surface remains hydrophilic.

A picture of the microsystem is reported in Fig. 1(a). The dispersed phase is injected in the microsystem's centre and flows through four one-dimensional arrays of microchannels, thus defining four production lines which each occupies a quarter of a circle. The latter are radially arranged in a circle whose centre matches that of the wafer. The mean height h of the shallow microchannels is 2 μm and the standard deviation is 0.1 μm, leading to a coefficient of variation of 5%. Each

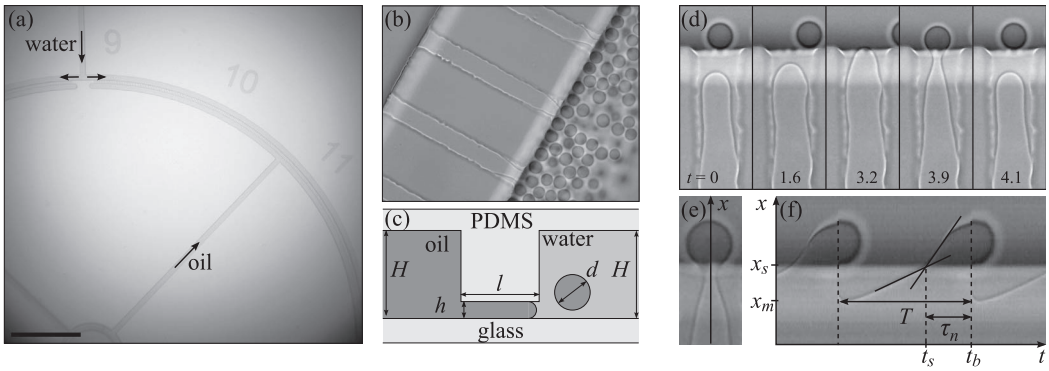

FIG. 1. (a) Large view of a one-dimensional membrane made of 1000 microchannels. The scale bar is 2 mm. (b) Close view of drop formation at microchannel's end. The channel width w is 10 μm. (c) Schematic of the membrane cross section along with the main parameters of the microfluidic system. Here, $h = 2\,\mu$m, $H = 20\,\mu$m, and $l = 100\,\mu$m. (d) Time sequence of drop formation. Time is indicated in ms. (e) Snapshot of the liquid finger at the step. (f) Spatiotemporal diagram built from an image sequence as reported in (d) along the axis x shown in (e) from which the characteristic time scales of drop formation are measured.

microchannel array is connected to a deep channel, where the continuous phase flows and carries away the droplets, with a width W of 150 μm and a height H of 20 μm (Fig. 1(b)). All production lines are composed of 252 parallel microchannels having a width w of 10 μm, a length l of 100 μm, and spaced by 50 μm (Fig. 1(c)). The liquid injection is either driven with syringe pumps (PHD 2200, Harvard Apparatus) or pressure control systems (MFCS-100, Fluigent). The drop formation dynamics is observed with a high speed camera (SA3, Photron) mounted on an inverted microscope. The drop size is evaluated from image processing.

The continuous aqueous phase is prepared from ultra pure water with sodium dodecyl suflate (SDS, Sigma). The viscosity of the continuous phase η_0 is tuned by adding a polymer, Polyethylene Glycol (PEG 3350, Sigma), at various concentrations up to 0.35 wt.% that corresponds to $\eta_0 = 26$ mPa s at 25 °C.[32] The dispersed phase is either a fluorocarbon oil (FC-3283, FC-40, and FC-70, 3M Fluorinert), a mineral oil (M8410, Sigma), or silicone oils (DC 200, Sigma). Their bulk properties are reported in Table. I. The surface tension γ between these oils and water with SDS at 1 wt.% is also given in Table. I. We note that the critical micellar concentration is found to be around 0.2 wt.% whatever the oil used. The interfacial tension is measured with a commercial apparatus (SA100, Krüss).

The flow in the microchannels is a Stokes one since the Reynolds number $R_e = \rho u_i h/\eta$ built from either the dispersed phase or the continuous one and where u_i is a characteristic velocity based on droplet size d and frequency f of droplet production, i.e., $u_i = \pi d^3 f/6hw$, is lower than 10^{-3}. This is also the case during the final stage of drop formation that is driven by capillarity and where the corresponding capillary number $C_a = \eta_i u_i/\gamma$, built on the inner phase properties, is smaller than 10^{-2}. The corresponding Weber number $W_e = \rho u_i^2 h/\gamma$ is also low, i.e., $W_e < 10^{-3}$. Concerning the shear force exerted on the forming drop by the outer phase flow, a modified capillary number

TABLE I. Properties of the dispersed phases at 25 °C where γ is the interfacial tension between the oils and an aqueous solution of SDS at 1 wt.%.

	η_i (mPa s)	ρ_i (kg/m^3)	γ (mN/m)
FC-3283	1.4	1820	18.8
FC-40	3.4	1850	18.8
FC-70	24	1940	19.4
Mineral oil	30	850	10.0
Silicone oil 50	50	960	9.0
Silicone oil 100	100	960	9.0

$C_a^o = \eta_o u_o d/\gamma h$, where u_o is a characteristic velocity of the outer phase, must be considered. Indeed, the drag force scales with the drop size d and the capillary force that keeps the growing drop attached to liquid finger is proportional to the microchannel height h (see Sec. III for more details). Only low shear regime, where $C_a^o < 10^{-1}$, has been investigated in the present work. The Bond number $B_O = \Delta\rho g d^2/\gamma$, defined from droplet size and where $\Delta\rho = |\rho_i - \rho_o|$, is at most equal to 5×10^{-5}. The effect of gravity is thus negligible during drop formation. This is not the case when droplets are flowing into the deep collecting channel which either quickly sediment or slowly cream because of a strong and weak density contrast, respectively (Table I).

III. DYNAMICS OF A SINGLE DROPLET GENERATOR

A. General observations

The emulsification features are first evaluated at the level of a single drop generator which is located at the beginning of a production line. A time sequence showing the emulsification process is reported in Fig. 1(d). The tip of the dispersed phase finger is moving back and forth in the shallow microchannel during drop formation. When approaching the end of the microchannel, the velocity of the finger tip is constant and increases linearly with the inner pressure p_i as expected for a Poiseuille flow. Then, the finger tip is accelerating at the step once the tip curvature drops down because of the vertical confinement release.[19,33] This motion leads to a stretching of the finger and the formation of a neck that eventually breaks up. The characteristic timescales of this phenomenon are measured from spatiotemporal diagrams as the one shown in Fig. 1(f). The oil finger reaches the step at time t_s which is determined by the intersection of the two tangents of the finger tip trajectory in the microchannel and just after the step. Then it breaks at time t_b, defining a necking time $\tau_n = t_b - t_s$. This process is periodically repeated with a time period T. The period of drop formation, the necking time as well as the corresponding drop size d are reported in Fig. 2 as a function of the inner pressure p_i at a fixed outer pressure p_o when mineral oil is used. We observe that all these parameters suddenly increase above a critical pressure p_i^*, here equal to 1.8×10^5 Pa. This transition has been found[20,21] to correspond to a critical capillary number C_a defined by the dispersed phase properties, i.e., $C_a = \eta_i u_i/\gamma$. Above this transition, the size polydispersity may remain below 1% (for most of the oils used here) or jump to multimodal size distributions (observed with FC-70) as in a dripping faucet regime.[34,35] From the pictures taken prior to the pinch-off and reported in Fig. 2(b), we note that when p_i is raised the location of the neck at breakup is further pushed downstream up to the step at the transition. This is in contrast to recent observations[19] made with channels having sizes 100 times larger and an aspect ratio equal to 2 where the breakup is located far from the step and moves

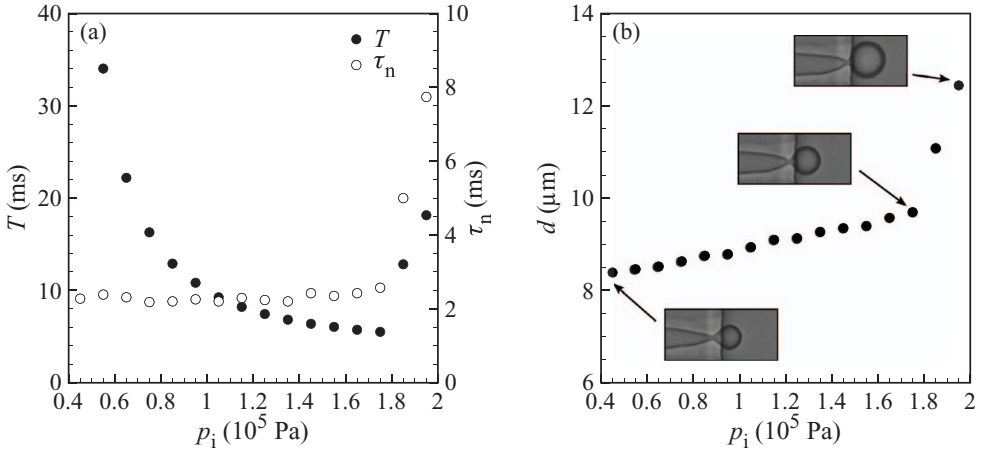

FIG. 2. (a) Evolution of the period of drop formation T (•) and the necking time τ_n (○) as a function of the inner pressure p_i for a constant outer pressure p_o set to 10^5 Pa for mineral oil in water. (b) Corresponding drop size d along with snapshots of the liquid finger prior to its breakup at various p_i.

further upstream for lower inner flow rates, a situation that ultimately affects drop size. Finally, we observe oscillations of the neck diameter before breakup in the large drop regime. This transition will be discussed in a Sec. III D.

Below p_i^*, T is obviously a decreasing function of p_i as it is inversely proportional to the dispersed phase flow rate q_i that is an increasing function of p_i. We then note that τ_n is constant, equal to 2.3 ms here, and then becomes an increasing function of p_i above the same critical pressure p_i^*. This is rather different from early observations[20] where τ_n slightly diminishes prior to the sudden rise. On the other hand, the drop size is a bit inflating before the transition as previously noticed.[19,20] The size increases linearly as a function of p_i with a slope equal to 10^{-5} μm Pa^{-1}.

The fact that τ_n is constant might arise from the mechanical properties of the material used in the present work for making the microsystems. Indeed, PDMS is an elastomer that easily deforms under pressure because of its moderate elastic modulus E close to 4 MPa.[36] For small deformation, the variation δh of the channel height is expected to vary like $\delta h \sim w p_i / E$.[37] On the other hand, the previous experiments on microchannel emulsification have been performed with stiff materials such as glass or silicon.

In order to investigate the link between mechanical properties of the present microsystem and the emulsification features, one has to precisely know the pressure at the step where drops are formed. Our strategy is thus to minimize the pressure drop of the inner phase due to the viscous resistance to flow in order to assume that the pressure at the step is the one at the feeding reservoir, i.e., p_i, and to finally correlate this pressure to channel deformation. For allowing the inner phase to invade the microchannel that links the two deep reservoirs, the inner pressure should overcome the Laplace pressure p_c given by $\gamma(2/h + 2/w)$, where h and w are the microchannel height and width, respectively (Fig. 1(c)). For a given inner pressure p_i, this condition is obtained by finding the critical outer pressure above which the finger tip does not move anymore, i.e., at the capillary pressure threshold. We remind that the pressures reported here are the controlled ones at the feeding reservoirs. Unfortunately, the pressure drop and thus the pressure at the microchannel end are not known *a priori* since the hydraulic resistance of the microsystem is modified by the presence of the emulsion droplets, especially at high volume fractions. Therefore, the pressure difference $p_i - p_o$ is not constant. When the pressure difference at the step is just above the capillary pressure threshold, the emulsification process is characterized by long periods of drop formation T, around 0.2 s, and thus to weak flow rates $q_i = \pi d^3/6T$ of the order of 10^{-15} m^3 s^{-1}. For a rigid microchannel, the corresponding pressure drop $b\eta_i l q_i / w h^3$, where $b = 13.7$ here,[38] is negligible since it is of the order of 10^3 Pa and moreover should decrease since the channel is deformed.[37]

The necking time τ_n and the corresponding drop size d_0 are reported in Fig. 3. Both increase linearly with p_i. The size $d_0 = d_0(0) + k_1 p_i$, where $d_0(0) = 7.8\,\mu$m and $k_1 = 1.4 \times 10^{-5}$ μm/Pa,

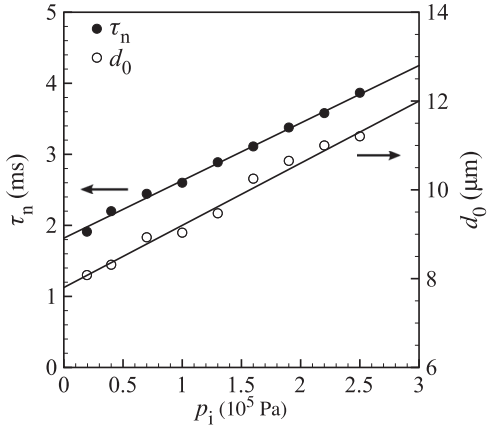

FIG. 3. Necking time τ_n (•) and the corresponding drop size d_0 (○) measured for various (p_i, p_o) couples by setting p_i just above the capillary pressure threshold, i.e., when $\tau_n/T \ll 1$, for mineral oil in water. The increase of τ_n and d_0 is a signature of PDMS wall deformation under pressure.

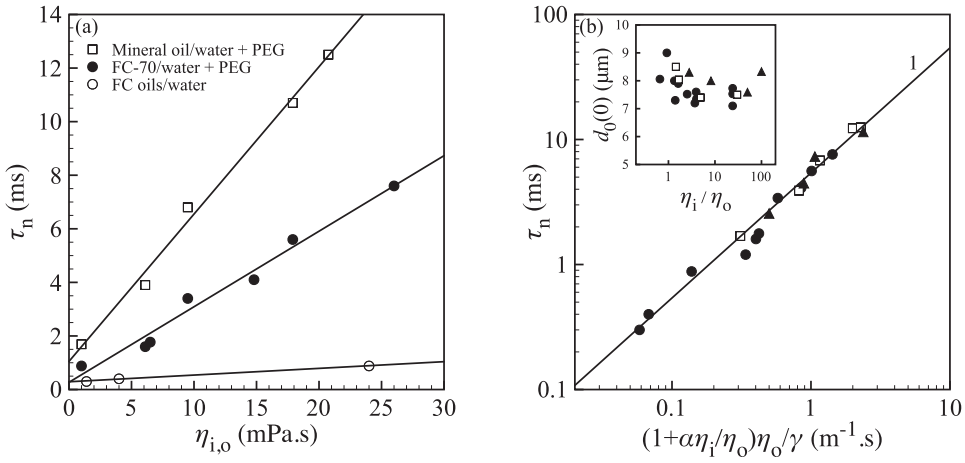

FIG. 4. (a) Evolution of the necking time as a function of the outer phase viscosity measured with mineral oil (□) or FC-70 oil (●) in PEG solutions at different concentrations, and as a function of the inner phase viscosity obtained with various fluorocarbon oils in water (○). (b) Necking time versus the inverse of a modified capillary velocity $\gamma/(1+\alpha\eta_i/\eta_0)\eta_0$ where $\alpha = 7\times10^{-2}$, for all formulations: FC oils (●), mineral oil (□), and silicone oils (▲). The continuous line represents a pure linear function. (Inset) minimal drop size against viscosity ratio.

represents the smallest drop size that can be created from this step emulsification process at a given channel height that is linked to the pressure at the step which is here assumed to be equal to p_i for this pressure setting. For a fixed p_o value, the drop size then increases for higher p_i and thus larger q_i as discussed later on in Sec. III C. As previously reported,[39,40] there exists a linear dependence between the drop size and the microchannel height, i.e., $d_0 = k_2 h = k_2(h_0 + \delta h)$ where h_0 is the channel height without any deformation. By considering the linear relationship between d_0 and p_i, one finds that $k_2 = d_0(0)/h_0 = 3.9$ and $\delta h = k_1 p_i/k_2$. Since $\delta h \sim w p_i/E$,[37] k_1/k_2 should correspond to w/E. For an elastic modulus E of 4 MPa and $w = 10$ μm, one gets $w/E = 2.5 \times 10^{-12}$ m/Pa which is in good agreement with $k_1/k_2 = 3.6\times10^{-12}$ m/Pa. The evolution of d_0 with p_i is thus consistent with a linear elastic deformation of the top wall made in PDMS. The fact that τ_n is also proportional to p_i and thus to h surprisingly makes τ_n independent of p_i for a fixed p_0, as reported in Fig. 2(a), and not slightly decreasing as previously observed.[20].

In the following, we then discuss about the effect of the formulation (η_i, η_o, γ) on the emulsification process features (τ_n, d_0) by considering their values extrapolated at $p_i = p_c = [0.12-0.24]$ 10^5 Pa, i.e., with negligible wall deformation and thus for a similar channel height.

B. Necking time

The evolution of the necking time as a function of either the outer phase viscosity η_o, obtained for mineral oil and FC-70 oil in various PEG solutions, or the inner phase viscosity η_i, obtained with three different fluorocarbon oils in water, is reported in Fig. 4(a). As expected, the characteristic time scale of the liquid finger breakup increases with the viscosity that sets the rate of dissipation during the pinch-off. This rise is found to be linearly dependent on the viscosity. The slowing down of the breakup dynamics is here principally ruled by the outer phase viscosity since the slope between τ_n and η_o is one order of magnitude larger than with η_i. This is a similar feature to the confined motion of bubbles[41] or drops[42,43] in tubes where dissipation in the lubrication film sets bubble or drop velocity. Moreover, since it is a capillary driven phenomenon, we note a two-fold reduction of the necking time between mineral oil and FC-70 oil that posses a rather close viscosity but the interfacial tension between water and fluorocarbon oil is almost two times larger than between water and mineral oil. We therefore propose the following semi-empirical evolution for τ_n:

$$\tau_n = a\left(1+\alpha\frac{\eta_i}{\eta_0}\right)\frac{\eta_0}{\gamma}, \quad (1)$$

where the constant a has the dimension of a length and α is a dimensionless constant. The necking time is plotted in Fig. 4(b) against $(1 + \alpha\eta_i/\eta_o)\eta_o/\gamma$, that can be assimilated to an inverse modified capillary velocity, for various oils and aqueous solutions of different viscosities corresponding to a viscosity ratio η_i/η_o that ranges from 0.65 to 100. A linear relationship is observed with $a = 10^{-3}$ m and $\alpha = 7 \times 10^{-2}$. The length a should contain the dependence of the characteristic timescale of the liquid finger breakup on the channel geometry, i.e., h and w, but this dependence remains to be elucidated.

In addition, the drop size $d_0(0)$ extrapolated to minimal pressure condition and thus to negligible wall deformation is reported in the inset plot of Fig. 4(b) as a function of the viscosity ratio. The minimal drop size is found to be rather independent of the formulation for $\eta_i/\eta_o > 1$, as previously reported,[44] and around 8 μm. We now wonder how the drop size vary with the flow conditions.

C. Drop size

As seen in Fig. 2(b) and previously reported,[19,20] when the pressure p_i is raised the drop size slightly increases prior to the transition to another fragmentation regime that leads to much larger drops. The drop inflation from its minimal volume $\mathcal{V}_0$ is attributed to the volume injected during the liquid finger breakup, i.e., during τ_n. The drop volume $\mathcal{V}_d$ is thus

$$\mathcal{V}_d = \mathcal{V}_0 + \int_{t_s}^{t_b} q_i(t)dt = \mathcal{V}_0 + q_i'\tau_n, \tag{2}$$

where q_i' is the average flow rate of the dispersed phase during drop formation at the step. We remind that here the pressure difference is imposed and the flow rate q_i is thus a function of time since the finger tip curvature is not constant with time. This flow rate is proportional to the overall average flow rate deduced from the drop volume $\mathcal{V}_d$ and period T, i.e., $q_i' = \beta\mathcal{V}_d/T$. The drop size d is finally given by

$$\frac{d}{d_0} = \left(1 - \beta\frac{\tau_n}{T}\right)^{-1/3}. \tag{3}$$

For the experiments reported in Fig. 2(b), the drop size increases by almost 20% when τ_n/T goes up to 0.5. This inflation is in accordance with Eq. (3) when $\beta = 0.8$. Unfortunately, the drop size augmentation is also affected by PDMS wall deformation when pressure is raised as shown in Fig. 3. Using stiffer materials should allow to cancel out this artifact while keeping the inflation process as it has been observed in silicon and glass devices[45,46] or from numerical simulations.[27]

D. Transition between two emulsification regimes

As previously reported,[20] there exists a transition of emulsification regime when the flow rate of the dispersed phase is raised and for which drop size suddenly increases. In the present experiments, this transition occurs at a critical pressure of the dispersed phase (Fig. 2). The value of this critical inner pressure is obviously a function of the outer phase pressure since it sets the local flow rate in the microchannel. We notice that, for a given formulation, the ratio between the necking time τ_n and the period of drop formation T^* at the transition is independent of the pressure conditions. On the other hand, this critical timescale ratio is found to be a function of the viscosity ratio and independent of interfacial tension. As shown in Fig. 5, the relationship between the two ratios is well represented by a power law

$$\frac{\tau_n}{T^*} = \left(\frac{\eta_i}{\eta_0}\right)^{-0.2}. \tag{4}$$

This relationship should be considered as an asymptotic limit for $\eta_i/\eta_0 > 1$ since τ_n cannot be larger than T^*. The transition has been described in term of a critical capillary number C_a^* built from the dispersed phase properties, i.e., $C_a^* = u_i\eta_i/\gamma$. By using Eqs. (1) and (4), the critical capillary number

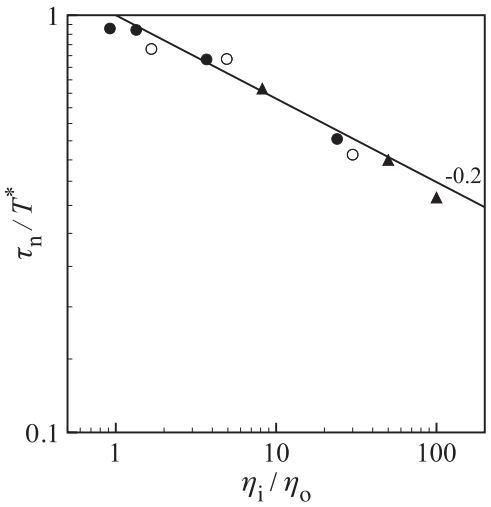

FIG. 5. Critical ratio between the necking time and the period of drop production that sets the transition from small to a large drop formation regime as a function of the viscosity ratio for various formulations: FC-70 (•), mineral oil (○), and silicone oils (▲). The continuous line represents a power-law function with an exponent of −0.2.

C_a^* at the transition, for $\lambda = \eta_i/\eta_0 > 1$, is given by

$$C_a^* = \frac{\pi}{6}\frac{d_0^3}{hwa}\frac{\lambda^{0.8}}{(1+\alpha\lambda)(1-\beta\lambda^{-0.2})}. \quad (5)$$

We remind that the length scale a should reflect the dependence of the necking time on microchannel height and width. We cannot directly compare Eq. (5) to our present data since the channel height, and therefore the inner phase velocity, is *a priori* unknown because of elastic deformation. According to Eq. (5), for given microchannel geometry and viscosity ratio, the transition between the two regimes of emulsification occurs at a constant capillary number C_a^*. This is in agreement with the original observations of Sugiura and co-workers.[20] In addition, C_a^* is a non-monotonous function of the viscosity ratio that initially increases twofold when λ is raised from 1 to 30, where β is taken here to be equal to 0.8 as previously estimated (Sec. III C), and then slightly decreases by almost 50% when λ is further raised from 30 to 1000. Of course, working with microsystems made from stiff materials would allow to precisely estimate β and thus the evolution of C_a^* with λ. However, this trend is consistent with previous observations made by Priest and co-workers[21] where, for a given liquid finger width, the critical capillary number is larger for a higher inner phase viscosity for which $\lambda = 9$.

IV. DYNAMICS OF A COLLECTION OF DROPLET GENERATORS

When an ensemble of microchannels are connected to a large and deep channel, where the continuous phase is flowing in a transverse direction, a droplet boundary layer develops along the droplet generators (Fig. 6(a)). As reported in Fig. 6(b), the thickness of this droplet boundary layer at a given location can be tuned by varying the outer pressure p_o for a fixed p_i. Here, the maximum p_o corresponds to the largest pressure above which the first microchannel of the array does not produce droplets anymore. We wonder if the features of the step-emulsification process is influenced or not by the cross-flow of such an emulsion.

A. Droplet production rate

The drop size is measured with a high precision at the first microchannel of a production line but this accuracy is altered along an array of microchannels because of close neighboring droplets. Therefore, only the drop size distributions, measured off chip, are discussed here. Alternatively, the

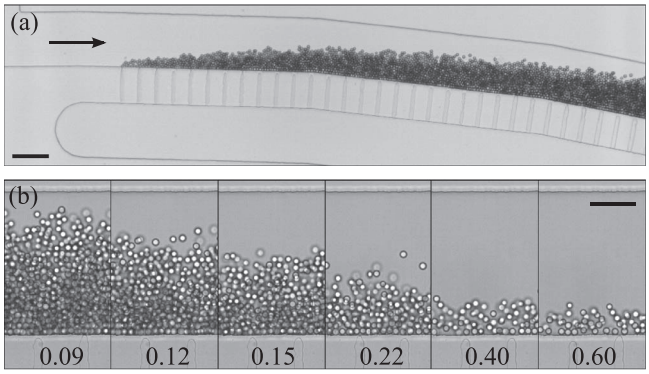

FIG. 6. (a) Development of a droplet boundary layer along the array of microchannels. The arrow indicates the water flow direction and the scale bar represents 100 μm. (b) Evolution of the droplet boundary layer at the end of a production line as a function of the outer pressure p_o, indicated in 10^5 Pa, for a fixed inner pressure set to 0.6×10^5 Pa. The scale bar represents 50 μm. The dispersed phase is mineral oil.

frequency of drop formation f, linked to the drop size *via* the inner flow rate by mass conservation, i.e., $q_i = \pi d^3 f/6$, can be correctly measured for all the drop makers. Here, only the small drop formation regime is discussed. The evolution of f, measured for a fixed inner pressure and two outer pressures, is reported in Fig. 7(a) as a function of the microchannel number that reflects its position along the production line. For the lowest outer pressure, i.e., for $p_o = 10^5$ Pa, we note that f oscillates around a constant value close to 270 Hz. On the other hand, for a higher p_o that leads to a thinner droplet layer, the frequency slightly increases while oscillating in phase with the other pressure condition. The synchronized modulations are a signature of microchannel height inhomogeneities and thus of a hydraulic resistance variability.

The influence of the outer pressure, and thus of the droplet boundary layer thickness, on the frequency of drop formation is reported in Fig. 7(b) at three locations along the one-dimensional membrane. The frequency at the first drop maker is obviously linearly decreasing when p_o is raised since the inner flow rate q_i is proportional to the pressure difference between the two phases and p_i is kept fixed. Then, the slope is lowered for a microchannel located at the middle of the production line. This is consistence with a pressure drop along the deep cross channel that, for a constant inner pressure, leads to an enhancement of the local flow rate q_i and thus f since the drop size d is moderately altered (Fig. 2(b)). Finally, the last drop maker produces droplets at a frequency that slightly increases with p_o. This counterintuitive phenomenon is a signature of an extra hydraulic

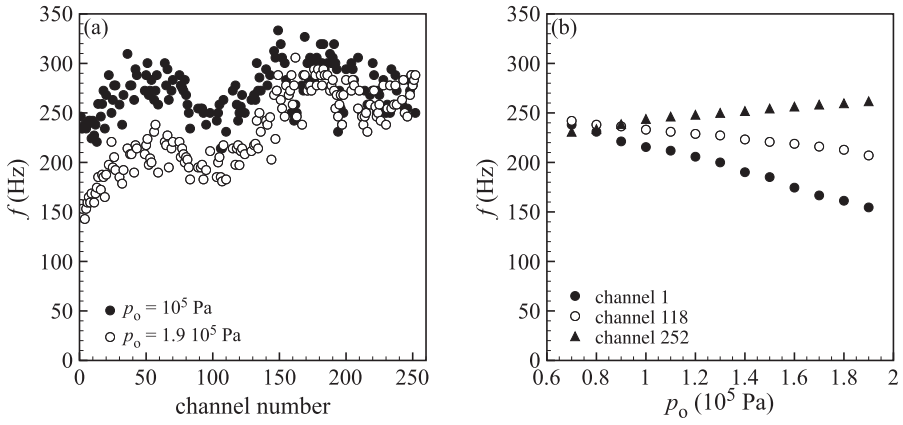

FIG. 7. (a) Frequency of drop formation as a function of the generator location for a given inner pressure $p_i = 10^5$ Pa and two outer pressures, 10^5 Pa (●) and 1.9×10^5 Pa (○). (b) Evolution of the frequency of drop formation as a function of p_o for $p_i = 10^5$ Pa at the beginning (●), at the middle (○), and at the end (▲) of the production line. The dispersed phase is FC-70.

resistance added by the compact emulsion. Indeed, far from the transition to a large drop regime, the period of drop formation is mainly linked to the time needed for the liquid finger to travel from its minimum location x_m to the step x_s (Fig. 1(f)) and therefore to the flow of the continuous phase in the microchannel and through the compact emulsion that can be seen as a porous medium.

This phenomenon directly impacts on the features of the final emulsion. Because there is a correlation between drop size and period of drop formation (Eq. (3)), working in a dilute regime, that corresponds to high p_o and where the frequency of drop formation varies along the production line, results in the larger size polydispersity. Indeed, the coefficient of variation of the frequency, defined as the ratio between the standard deviation and the mean value, is 17 % at $p_i = 1.9 \times 10^5$ Pa and drops down to 9% at $p_i = 10^5$ Pa and the corresponding size polydispersity is then 8.2% and 6.5%, respectively. The best polydispersity of such a membrane is one order of magnitude larger than a single microchannel and it is thus correlated to size heterogeneities among the vast number of microchannels. We stress here that the performance of the present microsystem made from soft lithography techniques is not so far from the one achieved in silicon and glass devices.[20]

As previously discussed, the maximum flow rate of the dispersed phase prior to the transition of fragmentation regime, from small to large droplet size, decreases when the inner viscosity increases or the interfacial tension is reduced. This impacts on the maximum production rate of fine and calibrated droplets with such a parallelization of drop formation. For example, the maximum production rate of FC-70 drops in water is 0.3 ml of droplets in 1 h that corresponds to the production of almost 10^9 droplets having a diameter of 9 μm in 1 h. For FC-3283 oil, a less viscous oil with the same interfacial tension, the maximum production rate is limited by the mechanical stability of the PDMS device and is equal to 4 ml of droplets per hour, i.e., about 10^{11} droplets in 1 h. In addition, because of microchannel height inhomogeneities, the transition is not observed at the same pressure conditions for all the droplet generators. This non-synchronization thus leads to size polydispersity of the final emulsion.

B. Droplet collision

Let us now investigate if the collision between flowing droplets and forming droplets may alter or not the emulsification dynamics. As previously mentioned, for an isolated droplet generator at a given pressure condition, the necking time is stable whatever the emulsification regime. On the other hand, while τ_n is also stable in a small drop formation regime for a downstream microchannel, the necking time start to fluctuate in the large drop formation regime and thus drop size polydispersity

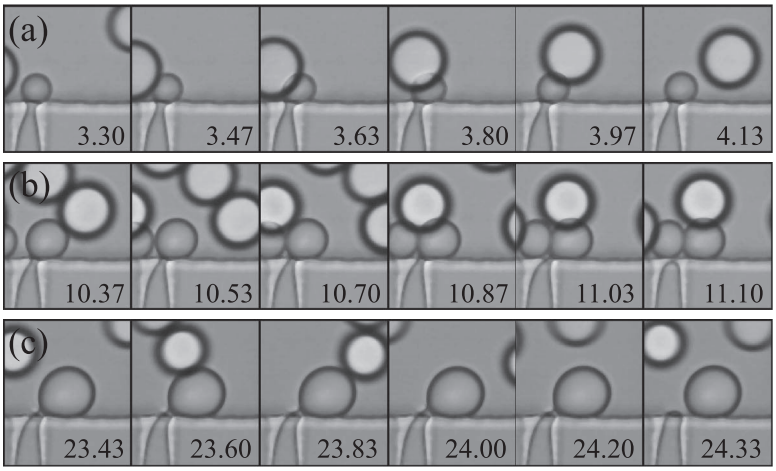

FIG. 8. Time sequences showing the collision between a flowing drop and a growing drop without fragmentation (a), a head-on collision that induces breakup (b) and a glancing collision that triggers breakup. Time is indicated in ms with $t = 0$ corresponding to the former breakup time. The dispersed phase is mineral oil injected at a pressure p_i of 3×10^5 Pa and the flow rate of the continuous phase is set to 1.4 ml/h.

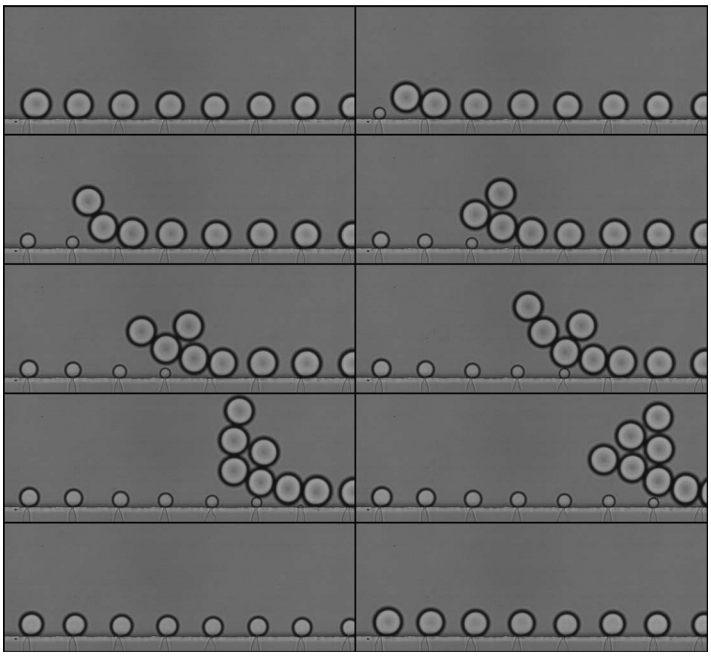

FIG. 9. Avalanche of collision-induced breakup events when all the droplet generators are working in a large drop formation regime. The snapshots show the first eight microchannels of the production line. The resulting drop diameter is 29 μm.

increases. As demonstrated in Fig. 8, where time sequences of the collision between flowing droplets and a growing one are reported, the droplets produced upstream are responsible of these fluctuations. Three different cases are identified. First, there is a critical size of the growing droplet below which the inflation process is not influenced by the other droplets (Fig. 8(a)). Then, two scenarios of collision-induced breakup are possible. If the upstream droplet is flowing against the wall where the microchannels emerge onto, a head-on collision is observed. This type of collision is efficient for triggering the fragmentation of the liquid finger and may lead to the formation of rather small drops (Fig. 8(b)). On the other hand, if there is an offset between the flowing drop and the growing one, a glancing collision occurs. In that case, breakup is observed only for larger inflating drops where the bridge that links the liquid finger to the emerging drop is stretched when the flowing drop is moving away (Fig. 8(c)). This is reminiscent to the collision of two drops in a shear flow[47] that may lead to coalescence.[48,49] The complete description of such a collision-induced breakup is beyond the scope of the present work. Further investigations are needed to evaluate the effect of the flowing drop size, velocity, and its distance to the wall, as well as the presence of other drops, on this phenomenon.

Finally, as shown in Fig. 9, we notice an avalanche event when all the droplet generators are working in a large drop regime. Indeed, the formation of the first drop triggers the detachment of the second one upon collision and so forth. This cascade maintains a phase between two neighboring drop makers that lead to the formation of a rather well monodisperse emulsion.

V. CONCLUSION AND PERSPECTIVES

The dynamics of step emulsification from a single to an array of drop generators has been investigated by using a microsystem realized by soft lithography technique. A scaling relationship between the intrinsic timescale of drop formation, namely, the necking time, and the fluid properties has been established, i.e., $\tau_n \sim (1 + \alpha\eta_i/\eta_o)\eta_o/\gamma$. Here, only one geometry of the microchannels has been considered. The microchannel height h sets the order of magnitude of the droplet diameter that is roughly four times h. The final drop size is modified by the dispersed phase flow rate through an inflation process where the necking time plays a major role. Unfortunately, because part of the microsystem is made with an elastomer, the microchannel walls are deformed under pressure and

thus the channel height is not known *a priori*. A natural follow up is to perform experiments by using stiffer materials like glass or polymers such as thiolene based resins.[50,51] The step emulsification process is known[20] to experience a transition between the formation of small drops to much larger drops. We show that this transition occurs at a critical ratio between the necking time and the period of drop formation that scales with the viscosity ratio λ of the two phases like $\lambda^{-0.2}$ for $\lambda > 1$. This scaling leads to a correction of the critical capillary number, based on the dispersed phase properties, in agreement with previous observations.[20,21] We stress that a theoretical description of this peculiar transition of fragmentation regime is still lacking. We then studied the emulsification process of an array of microchannels with a cross flow of the continuous phase, a situation relevant for making large amounts of emulsion droplets for further applications. When all the drop generators are working in a small drop regime, a droplet boundary layer develops against the array of microchannel. This compact emulsion is shown to lead to an homogenization of the droplet production rate of the drop makers thanks to an extra hydraulic resistance imposed by the dense stack of droplets. This phenomenon ultimately narrow the drop size distribution of the final emulsion. While the emulsification dynamics in the small drop formation regime is not influenced by the flow of the upstream formed droplets, collision-induced breakup has been observed in the large drop formation regime. This event finally led to polydisperse emulsions. Further investigations are needed to evaluate the effect of the flowing drop size, velocity, and its distance to the wall, as well as the presence of other drops, on this phenomenon. Microfluidics offers an unique tool for exploring emulsions properties[52] as well as their formation mechanisms. Indeed, such a configuration, where the drop generators are set on a plan, offers a complementary approach to microfabricated membranes in silicon[53–56] for investigating the membrane emulsification process for which the step-emulsification phenomenon does not occur, i.e., for $h/w < 3$, and where shear and droplet-droplet interaction play a crucial role.

ACKNOWLEDGMENTS

This work is supported by a public grant overseen by the French National Research Agency (ANR) as part of the Investissements dAvenir program (Reference No. ANR-10-NANB-0002-06).

[1] F. Leal-Calderon, V. Schmitt, and J. Bibette, *Emulsion Science–Basic Principles* (Springer, New York, 2007).
[2] G. I. Taylor, "The formation of emulsions in definable fields of flow," Proc. R. Soc. Lond. A **146**, 501 (1934).
[3] T. G. Mason and J. Bibette, "Emulsification in viscoelastic media," Phys. Rev. Lett. **77**, 3481 (1996).
[4] E. Lucassen-Reynders and K. Kuijpers, "The role of interfacial properties in emulsification," Colloids Surf. **65**, 175 (1992).
[5] O. Olsvik, T. Popovic, E. Skjerve, K. S. Cudjoe, E. Hornes, J. Ugelstad, and M. Uhln, "Magnetic separation techniques in diagnostic microbiology," Clin. Microbiol. Rev. **7**, 43 (1994).
[6] M. Margulies, M. Egholm, W. E. Altman, S. Attiya, J. S. Bader, L. A. Bemben, J. Berka, M. S. Braverman, Y.-J. Chen, Z. Chen *et al.*, "Genome sequencing in microfabricated high-density picolitre reactors," Nature (London) **437**, 376 (2005).
[7] N.-B. Liabakk, K. Nustad, and T. Espevik, "A rapid and sensitive immunoassay for tumor necrosis factor using magnetic monodisperse polymer particles," J. Immunol. Meth. **134**, 253 (1990).
[8] T. Nakashima, M. Shimizu, and M. Kukizaki, "Particle control of emulsion by membrane emulsification and its applications," Adv. Drug Delivery Rev. **45**, 47 (2000).
[9] S. M. Joscelyne and G. Tragardh, "Membrane emulsification: A literature review," J. Membr. Sci. **169**, 107 (2000).
[10] G. T. Vladisavljevic and R. A. Williams, "Recent developments in manufacturing emulsions and particulate products using membranes," Adv. Colloid Interf. Sci. **113**, 1 (2005).
[11] R. A. Williams, S. J. Peng, D. A. Wheeler, N. C. Morley, D. Taylor, M. Whalley, and D. W. Houldsworth, "Controlled production of emulsions using a crossflow membrane. Part II. Industrial scale manufacture," Chem. Eng. Res. Des. **76**, 902 (1998).
[12] M. Yasuno, M. Nakajima, S. Iwamoto, T. Maruyama, S. Sugiura, I. Kobayashi, A. Shono, and K. Satoh, "Visualization and characterization of spg membrane emulsification," J. Membr. Sci. **210**, 29 (2002).
[13] T. Kawakatsu, Y. Kikuchi, and M. Nakajima, "Regular-sized cell creation in microchannel emulsification by visual microprocessing method," J. Am. Oil Chem. Soc. **74**, 317 (1997).
[14] I. Kobayashi, M. Nakajima, K. Chun, Y. Kikuchi, and H. Fukita, "Silicon array of elongated through-holes for monodisperse emulsion droplets," AIChE J. **48**, 1639 (2002).
[15] I. Kobayashi, S. Mukataka, and M. Nakajima, "Novel asymmetric through-hole array microfabricated on a silicon plate for formulating monodisperse emulsions," Langmuir **21**, 7629 (2005).
[16] S. Sugiura, M. Nakajima, S. Iwamoto, and M. Seki, "Interfacial tension driven monodispersed droplet formation from microfabricated channel array," Langmuir **17**, 5562 (2001).
[17] I. Kobayashi, S. Mukataka, and M. Nakajima, "Effect of slot aspect ratio on droplet formation from silicon straight-through microchannels," J. Colloid Interf. Sci. **279**, 277 (2004).

[18] G. T. Vladisavljevic, I. Kobayashi, M. Nakajima, R. A. Williams, M. Shimizu, and T. Nakashima, "Shirasu porous glass membrane emulsification: Characterisation of membrane structure by high-resolution x-ray microtomography and microscopic observation of droplet formation in real time," J. Membr. Sci. **302**, 243 (2007).
[19] R. Dangla, E. Fradet, Y. Lopez, and C. N. Baroud, "The physical mechanisms of step emulsification," J. Phys. D: Appl. Phys. **46**, 114003 (2013).
[20] S. Sugiura, M. Nakajima, N. Kumazawa, S. Iwamoto, and M. Seki, "Characterization of spontaneous transformation-based droplet formation during microchannel emulsification," J. Phys. Chem. B **106**, 9405 (2002).
[21] C. Priest, S. Herminghaus, and R. Seemann, "Generation of monodisperse gel emulsions in a microfluidic device," Appl. Phys. Lett. **88**, 024106 (2006).
[22] T. Kawakatsu, G. Tragardh, Y. Kikuchi, M. Nakajima, H. Komori, and T. Yonemoto, "Effect of microchannel structure on droplet size during crossflow microchannel emulsification," J. Surfactants Deterg. **3**, 295 (2000).
[23] G. T. Vladisavljevic, I. Kobayashi, and M. Nakajima, "Production of uniform droplets using membrane, microchannel and microfluidic emulsification devices," Microfluid. Nanofluid. **13**, 151 (2012).
[24] S. Sugiura, M. Nakajima, and M. Seki, "Prediction of droplet diameter for microchannel emulsification," Langmuir **18**, 3854 (2002).
[25] E. van der Zwan, K. Schroen, and R. Boom, "A geometric model for the dynamics of microchannel emulsification," Langmuir **25**, 7320 (2009).
[26] I. Kobayashi, S. Mukataka, and M. Nakajima, "Effects of type and physical properties of oil phase on oil-in-water emulsion droplet formation in straight-through microchannel emulsification, experimental and cfd studies," Langmuir **21**, 5722 (2005).
[27] E. van der Zwan, R. van der Sman, K. Schroen, and R. Boom, "Lattice boltzmann simulations of droplet formation during microchannel emulsification," J. Colloid Interf. Sci. **335**, 112 (2009).
[28] S. Sugiura, M. Nakajima, and M. Seki, "Effect of channel structure on microchannel emulsification," Langmuir **18**, 5708 (2002).
[29] I. Kobayashi, Y. Wada, K. Uemura, and M. Nakajima, "Microchannel emulsification for mass production of uniform fine droplets: integration of microchannel arrays on a chip," Microfluid. Nanofluid. **8**, 255 (2010).
[30] T. Kawakatsu, H. Komori, M. Nakajima, Y. Kikuchi, and T. Yonemoto, "Production of monodispersed oil-in-water emulsion using crossflow-type silicon microchannel plate," J. Chem. Eng. Jpn. **32**, 241 (1999).
[31] J. C. McDonald, D. C. Duffy, J. R. Anderson, D. T. Chiu, H. K. Wu, O. J. A. Schueller, and G. M. Whitesides, "Fabrication of microfluidic systems in poly(dimethylsiloxane)," Electrophoresis **21**, 27 (2000).
[32] P. Gonzalez-Tello, F. Camacho, and G. Blazquez, "Density and viscosity of concentrated aqueous solutions of polyethylene glycol," J. Chem. Eng. Data **39**, 611 (1994).
[33] R. Dangla, S. C. Kayi, and C. N. Baroud, "Droplet microfluidics driven by gradients of confinement," Proc. Natl. Acad. Sci. U.S.A. **110**, 853 (2013).
[34] C. Clanet and J. C. Lasheras, "Transition from dripping to jetting," J. Fluid Mech. **383**, 307 (1999).
[35] B. Ambravaneswaran, H. J. Subramani, S. D. Phillips, and O. A. Basaran, "Dripping-jetting transitions in a dripping faucet," Phys. Rev. Lett. **93**, 034501 (2004).
[36] D. Fuard, T. Tzvetkova-Chevolleau, S. Decossas, P. Tracqui, and P. Schiavone, "Optimization of poly-di-methyl-siloxane (pdms) substrates for studying cellular adhesion and motility," Microelectron. Eng. **85**, 1289 (2008).
[37] T. Gervais, J. El-Ali, A. Gunther, and K. F. Jensen, "Flow-induced deformation of shallow microfluidic channels," Lab Chip **6**, 500 (2006).
[38] C. J. Morris and F. K. Forster, "Oscillatory flow in microchannels - comparison of exact and approximate impedance models with experiments," Exp. Fluids **36**, 928 (2004).
[39] F. Malloggi, N. Pannacci, R. Attia, F. Monti, P. Mary, H. Willaime, P. Tabeling, B. Cabane, and P. Poncet, "Monodisperse colloids synthesized with nanofluidic technology," Langmuir **26**, 2369 (2010).
[40] L. L. Shui, A. van den Berg, and J. C. T. Eijkel, "Scalable attoliter monodisperse droplet formation using multiphase nano-microfluidics," Microfluid. Nanofluid. **11**, 87 (2011).
[41] F. P. Bretherton, "The motion of long bubbles in tubes," J. Fluid Mech. **10**, 166 (1961).
[42] A. Borhan and J. Pallinti, "Pressure-driven motion of drops and bubbles through cylindrical capillaries: Effect of buoyancy," Ind. Eng. Chem. Res. **37**, 3748 (1998).
[43] S. R. Hodges, O. E. Jensen, and J. M. Rallison, "The motion of a viscous drop through a cylindrical tube," J. Fluid Mech. **501**, 279 (2004).
[44] K. van Dijke, I. Kobayashi, K. Schroen, K. Uemura, M. Nakajima, and R. Boom, "Effect of viscosities of dispersed and continuous phases in microchannel oil-in-water emulsification," Microfluid. Nanofluid. **9**, 77 (2010).
[45] G. T. Vladisavljevic, I. Kobayashi, and M. Nakajima, "Effect of dispersed phase viscosity on maximum droplet generation frequency in microchannel emulsification using asymmetric straight-through channels," Microfluid. Nanofluid. **10**, 1199 (2011).
[46] M. Stoffel, S. Wahl, E. Lorenceau, R. Höhler, B. Mercier, and D. E. Angelescu, "Bubble production mechanism in a microfluidic foam generator," Phys. Rev. Lett. **108**, 198302 (2012).
[47] M. Loewenberg and E. J. Hinch, "Collision of two deformable drops in shear flow," J. Fluid Mech. **338**, 299 (1997).
[48] L. G. Leal, "Flow induced coalescence of drops in a viscous fluid," Phys. Fluids **16**, 1833 (2004).
[49] N. Bremond, A. R. Thiam, and J. Bibette, "Decompressing emulsion droplets favors coalescence," Phys. Rev. Lett. **100**, 024501 (2008).
[50] Z. T. Cygan, J. T. Cabral, K. L. Beers, and E. J. Amis, "Microfluidic platform for the generation of organic-phase microreactors," Langmuir **21**, 3629 (2005).
[51] D. Bartolo, G. Degre, P. Nghe, and V. Studer, "Microfluidic stickers," Lab Chip **8**, 274 (2008).
[52] N. Bremond and J. Bibette, "Exploring emulsion science with microfluidics," Soft Matter **8**, 10549 (2012).

[53] A. J. Abrahamse, R. van Lierop, R. G. M. van der Sman, A. van der Padt, and R. M. Boom, "Analysis of droplet formation and interactions during cross-flow membrane emulsification," J. Membr. Sci. **204**, 125 (2002).
[54] A. J. Gijsbertsen-Abrahamse, A. van der Padt, and R. M. Boom, "Status of cross-flow membrane emulsification and outlook for industrial application," J. Membr. Sci. **230**, 149 (2004).
[55] M. Geerken, R. Lammertink, and M. Wessling, "Tailoring surface properties for controlling droplet formation at microsieve membranes," Colloids Surf., A **292**, 224 (2007).
[56] E. Egidi, G. Gasparini, R. G. Holdich, G. T. Vladisavljevic, and S. R. Kosvintsev, "Membrane emulsification using membranes of regular pore spacing: Droplet size and uniformity in the presence of surface shear," J. Membr. Sci. **323**, 414 (2008).